Analytical Methods

TECHNICAL NOTE

View Article Online
View Journal | View Issue



Cite this: *Anal. Methods*, 2016, **8**, 7552

# Characterisation of matrix-based polyatomic interference formation in laser ablation-inductively coupled plasma-mass spectrometry using dried micro-droplet ablation and its relevance for bioimaging

Dominic J. Hare,*[ab] Fred Fryer,[c] Bence Paul,[d] David P. Bishop[a] and Philip A. Doble*[a]

Dried micro-droplets were used to characterise the formation of polyatomic interferences in a commercial laser ablation-inductively coupled plasma-mass spectrometer (LA-ICP-MS). Droplets containing 4 ng each of Al, As, Ca, Cd, Co, Cu, Fe, Mg, Mn, P, Se and Zn in the presence of potentially interfering isotopes were deposited on silicate microscope slides. Comparisons of the total signal recorded for each dried droplet showed no detectable influence of polyatomic matrix-based interferences. Visualisation of acquired signal was achieved by the generation of two-dimensional maps. The natural abundance pattern of elements with two measurable isotopes was confirmed for each droplet. The lack of interferences was due to the absence of major gas molecules (*e.g.* $N_2$, $O_2$, $CO_2$) from the laser cell and minimal total matrix load on the plasma when compared to standard solution nebulisation (approx. ng $s^{-1}$ *versus* 10–20 μL $s^{-1}$) ICP-MS conditions.

Received 10th September 2016
Accepted 1st October 2016

DOI: 10.1039/c6ay02545e

www.rsc.org/methods



## 1 Introduction

Laser ablation (LA) has greatly expanded the capability of conventional ICP-MS instruments, allowing for rapid analysis of trace elements *via* direct solid sampling.[1] In the biological sciences, LA-ICP-MS has also revolutionised spatial measurement and mapping of total metal distributions, providing an accessible alternative to synchrotron-based microprobes with more than adequate sensitivity for most biologically-relevant metals.[2]

It is often assumed that LA-ICP-MS suffers from significant isobaric interferences from polyatomic species[3] in line with traditional solution nebulisation (SN) ICP-MS. While it has been suggested that interferences, particularly those arising from water in the sample matrix, are considerably lower in LA-ICP-MS,[4,5] reduced interference formation in the context of bioimaging has not been confirmed. ICP-MS instruments with quadrupole mass filters typically have mass resolution of 0.1 atomic mass units. Therefore, polyatomic species with the same nominal mass as the ion of interest cause significant interfering signal that precludes accurate measurement. For SN-ICP-MS either a higher resolution mass filter (such as a sector field design[6]) or collision/reaction gas[7,8] is required to negate the effect of, or physically remove interferences. Sector field instruments command a considerably higher price than quadrupole instruments with minimal or even no increase in sensitivity and a more limited range of sequentially scanned isotopes.[9] Reaction/collision cell equipped quadrupole ICP-MS exhibit a significant drop in signal abundance (often by a factor of 10 or more), which is unfavourable when introducing comparatively smaller amounts of material to the plasma *via* LA.

Ablated analytes transported to the ICP-MS reach the plasma in a very different state when compared to SN. Most significantly, solvent-free particles of a much smaller diameter[10] are produced by commercially available UV lasers. The ablation process involves desorption, vapourisation and ionisation of the analyte and subsequent condensation and aggregation from the laser plasma to form laser aerosols.[11,12] Therefore, it is reasonable to assume that applying operational parameters similar to solution nebulisation is unnecessary in LA-ICP-MS to achieve adequate determination.

$MO^+$, $MN^+$ and $MH^+$ based interferences primarily arise from air ($N_2$, $O_2$ *etc.*) and the solvent in use (mainly $H_2O$ based matrices, along with $Cl^+$ and $N^+$ species in certain acidic matrices). These highly abundant ions are generated within the plasma,[13] and are somewhat controlled in solution nebulisation ICP-MS by manipulation of parameters that influence plasma

[a]*Elemental Bio-imaging Facility, University of Technology Sydney, PO Box 123, Broadway, New South Wales, Australia. E-mail: dominic.hare@uts.edu.au; philip.doble@uts.edu.au; Tel: +61 3 9035 9549; +61 2 9514 1792*

[b]*The Florey Institute of Neuroscience and Mental Health, The University of Melbourne, Parkville, Victoria, Australia*

[c]*Agilent Technologies Australia, Mulgrave, Victoria, Australia*

[d]*School of Earth Sciences, The University of Melbourne, Parkville, Victoria, 3052, Australia*

temperature such as carrier gas flow rate, radio frequency (RF) power; or residence time such as sampling depth, and to a lesser extent sampling cone orifice dimesions.[14] The degree to which these parameters can be controlled is limited, as adequate desolvation and ionisation is dependent on the duration the particle resides within the plasma and the applied power. The 'dry' nature of the plasma in LA-ICP-MS is advantageous, as the confounding effects of $H_2O$ and N on polyatomic interference from the typical acidic matrices used in solution nebulisation ICP-MS are significantly reduced. Reducing the potential for interference formation can sufficiently negate the need for post-plasma treatment, such as collision gases or high resolution mass filters.

Dried droplet ablation has been suggested as an alternative method to electrothermal vapourisation (ETV) ICP-MS for the discrete sampling of small volume aqueous samples.[15] Günther *et al.*[16] showed that direct ablation of dried solutions yielded no significant elemental fractionation. Dried droplet analysis was also shown to be suitable for the simultaneous determination of 21 isotopes with absolute detection limits in the sub ng $g^{-1}$ range.[5] Volumes as low as 20 μL have been used to quantify μg $g^{-1}$ concentrations of selenomethionine in yeast *via* droplet analysis of HPLC fractions.[17] It has also been shown that dried droplet analysis yielded a 100-fold decrease in hydride formation of radionucliotides when compared to both solution nebulisation and ETV-ICP-MS.[18] Ablation of dried blood droplets on filter paper has been suggested as a suitable technique for the measurement of Pb toxicity.[19] Recently, 5–20 μL droplets of acidified standard solutions placed on filter paper supports has been successfully used for multi-point external calibration in imaging experiments.[20]

The object of this study was to characterise interference formation in a commercial LA-ICP-MS instrument using dried sub-μL volume droplets. The experimental design was based on the theoretical formation of polyatomic isobaric interferences to determine the influence of matrix components on true analyte signal.

## 2 Materials and methods

### Instrumentation

A New Wave UP-213 laser ablation unit (Kenelec Scientific, Mitcham, Victoria, Australia) with a Nd:YAG laser emitting a 213 nm laser beam was used. The laser was hyphenated to an Agilent Technologies 7500ce ICP-MS (Mulgrave, Victoria, Australia) system fitted with 'cs' lenses for enhanced sensitivity. High purity liquid argon (Ace Cryogenic, Castle Hill, NSW, Australia) was used for all analyses. The system was tuned for sensitivity prior to all analyses using NIST 612 glass, with $^{7}Li$, $^{59}Co$, $^{89}Y$, $^{238}U$ and responses monitored. Oxide formation was monitored as the $^{232}Th^{+}/^{232}Th^{16}O^{+}$ ratio and was <0.3% for all experiments. High laser energy fluence can introduce contaminates from the underlying glass matrix, depending on the glass composition.[21] An average laser fluence of 0.15 J $cm^2$ and repetition rate of 20 Hz was used, which is well below the reported threshold for ablation of soda-lime glass (the major matrix of the support slides used; see below) for UV lasers of approximately 0.80–0.86

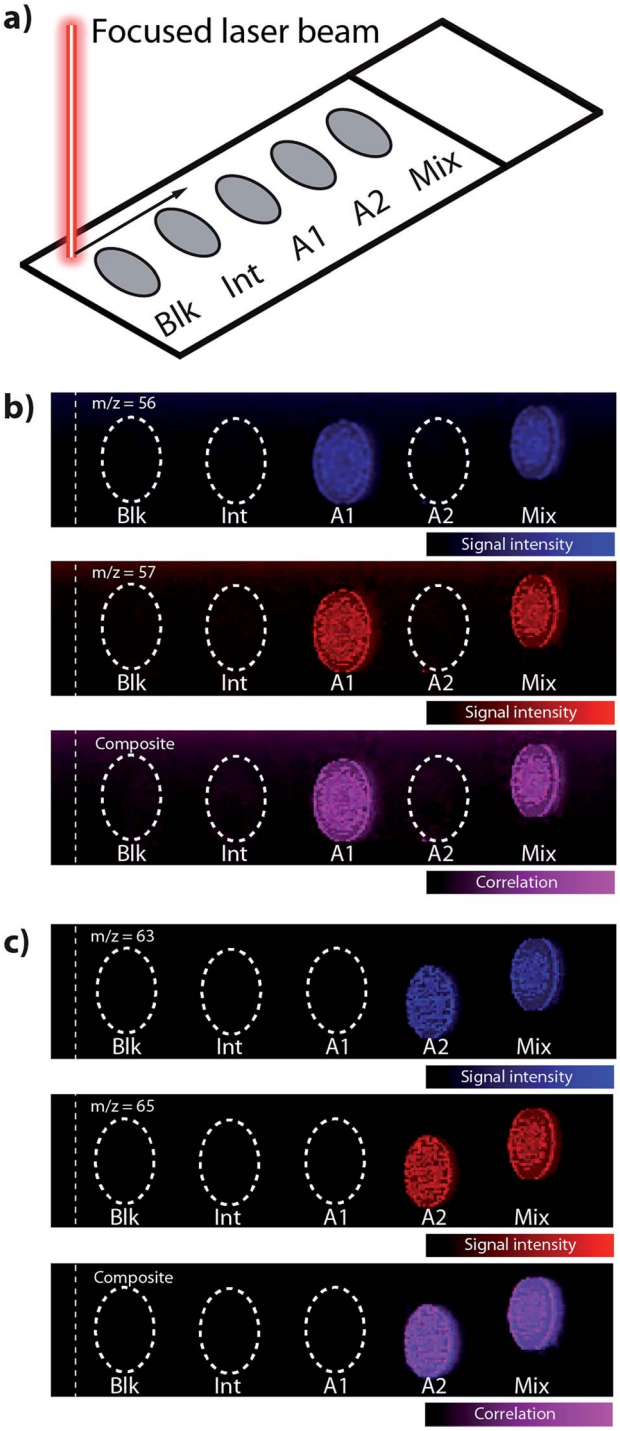


Fig. 1 (a) Schematic representation of imaging dried droplets on a standard microscope slide by LA-ICP-MS. (b and c) Relative intensity maps of iron (*m/z* 56, 57) and copper (*m/z* = 63, 65) in deposited droplets with corresponding composite images, showing negligible interferences on any measured mass due to theoretical polyatomic species (see Table 2). The area left of the dashed white line indicates the gas blank signal, showing no discernible increase in signal arising from potential $^{40}Ar^{16}O^{+}$ or $^{23}Na^{40}Ar^{+}$ interferences on $^{56}Fe$ or $^{63}Cu$, respectively.

J $cm^{-2}$.[22] For other support matrices, fluence should be selected based on the appropriate threshold of ablation for the material in question. Comparisons of the gas blank and ablated areas of the support slide only showed no discernible increase in Si and Na (the major elemental components of glass) signal (Fig. 1).

### Reagents and solutions

10 ± 0.2 mg $L^{-1}$ solutions of each element shown in Table 1 were used (Choice Analytical, Thornleigh, NSW, Australia). Solutions were made to mass using 1% Seastar Baseline grade $HNO_3$ (Choice Analytical) with approximately 10 μg $mL^{-1}$ amido black added to aide in visualisation of dried droplets.

### Deposition of droplets

0.4 μL of each solution (amounting to 4 ng of each element) was dropped directly onto high-purity KNITTEL StarFrost soda-lime glass microscope slides (ProSciTech, Townsville, Queensland, Australia) using a Gilson air displacement pipette. The solution was expelled to a point where a droplet formed on the pipette tip, and was then placed onto the slide surface. The slide was then allowed to dry in an enclosed desiccator prior to analysis.

Five solutions were prepared (see Table 1). These consisted of a blank solution containing only amido black and solutions containing potential interfering elements (a list of theoretical polyatomic interferences are listed in Table 2), analyte elements and a mixture of all elements used (Fig. 1a). The amido black was added to locate the dried spots using the CCD camera on the laser unit. The amido black was also a source of carbon to evaluate potential $^{12}C$ and $^{13}C$-based interferences. Nitrate from the 1% $HNO_3$ matrix remaining on the slide surface after drying provided a potential source of $^{14}N$-based interferences. Approximate total amounts of N, O and C from the nitrate anion and 10 μg $mL^{-1}$ amido black dye are 124 ng, 429 ng and 1.72 pg, respectively.

### Data processing

Each line of ablation in the *x*-axis produced a single data file in comma separated value (.csv) format. Using a Visual Basic macro in Microsoft Excel,[23] data was combined into a single ASCII file for importation into ENVI (Exelis Visual Information Solutions, Boulder, Colorado, USA). Droplet images were standardised to $^{13}C$ from the amido black according to methods previously described.[24] Raw count data was then extracted from ENVI by selecting the area of the droplet and exporting as a rich text format file. Mean background signal for each *m*/*z* was subtracted and the sum of raw counts for each droplet was tabulated and compared. Five replicate measurements of experiment were carried out. Composite images shown in Fig. 1b and c were produced in ImageJ, with Pearson correlation coefficients calculated using the 'Intensity Correlation Analysis' plugin.[25]

Table 1 Composition of interference (Int) and analyte-containing (A1, A2 and mix) solutions

| Solution | Metal contents[a] |
|---|---|
| Blank | — |
| Int | Ca, Co, K, Mo, Mg, Na (10 mg $L^{-1}$) |
| A1 | Al, As, Cd, Fe, K, Mg, P, Se (10 mg $L^{-1}$) |
| A2 | Ca, Cu, Zn, Mn (10 mg $L^{-1}$) |
| Mix | All |

[a] All solutions contained 10 μg $mL^{-1}$ amido black.

Table 2 Theoretical major polyatomic interferences. Adapted from May *et al.*[26]

| Analyte | Interfering species |
|---|---|
| $^{27}Al^+$ | $^{12}C^{15}N^+$, $^{13}C^{14}N^+$, $^{14}N_2{}^+$ spread |
| $^{75}As^+$ | $^{40}Ar^{35}Cl^+$, $^{59}Co^{16}O^+$, $^{36}Ar^{39}K^+$, $^{43}Ca^{16}O_2{}^+$, $^{23}Na^{12}C^{40}Ar^+$ |
| $^{43}Ca^+$ | $^{27}Al^{16}O^+$ |
| $^{44}Ca^+$ | $^{12}C^{16}O_2{}^+$, $^{14}N_2{}^{16}O^+$, $^{28}Si^{16}O^+$ |
| $^{111}Cd^+$ | $^{95}Mo^{16}O^+$ |
| $^{112}Cd^+$ | $^{40}Ca_2{}^{16}O_2{}^+$, $^{40}Ar_2{}^{16}O_2{}^+$ |
| $^{59}Co^+$ | $^{43}Ca^{16}O^+$, $^{24}Mg^{35}Cl^+$ |
| $^{63}Cu^+$ | $^{40}Ar^{23}Na^+$, $^{40}Ca^{23}Na^+$, $^{31}P^{16}O_2{}^+$ |
| $^{65}Cu^+$ | $^{40}Ar^{25}Mg^+$ |
| $^{56}Fe^+$ | $^{40}Ar^{16}O^+$, $^{40}Ca^{16}O^+$ |
| $^{57}Fe^+$ | $^{40}Ar^{16}OH^+$, $^{40}Ca^{16}OH^+$ |
| $^{24}Mg^+$ | $^{12}C_2{}^+$ |
| $^{25}Mg^+$ | $^{12}C_2H^+$ |
| $^{26}Mg^+$ | $^{12}C^{14}N^+$, $^{12}C_2H_2{}^+$, $^{12}C^{13}CH^+$ |
| $^{55}Mn^+$ | $^{40}Ar^{14}NH^+$, $^{39}K^{16}O^+$ |
| $^{31}P^+$ | $^{14}N^{16}OH^+$ |
| $^{78}Se^+$ | $^{40}Ar^{38}Ar^+$ |
| $^{80}Se^+$ | $^{40}Ar_2{}^+$ |
| $^{64}Zn^+$ | $^{32}S^{16}O_2{}^+$ |
| $^{66}Zn^+$ | $^{34}S^{16}O_2{}^+$, $^{40}Ar^{14}N_2{}^+$ |

## 3 Results and discussion

The optimised plasma operating conditions are summarised in Table 3. In typical solution ICP-MS measurement using the 7500ce system an RF power of 1500 W is applied to the plasma. Additionally, solution ICP-MS requires a sample depth of 6–8 mm to allow adequate ionisation of material. Lower plasma power (1200 W) results in less ionising potential of the plasma, with fewer energetic electrons available for ionising analyte. Additionally, the short residence time in the plasma due to decreased sample depth gives less opportunity for polyatomic species to form.[27]

A 5 × 30 mm area encompassing all deposited droplets was ablated to ensure all material was transported to the ICP. Analysis time was approximately four hours per sample set. Images for *m*/*z* 56 and 57 are shown in Fig. 1b. Correlation analysis of *m*/*z* 56 and 57 images showed a Pearson correlation coefficient of 0.979, indicating no additional signal above the background was recorded from one of the most prevalent polyatomic interference normally encountered, $^{40}Ar^{16}O^+$ on $^{56}Fe^+$. A background signal was present for *m*/*z* 56 when the laser was not operational, produced from trace $O_2$ impurities present in the argon gas. Furthermore, this background was

 

Table 3 LA and ICP-MS operating conditions

| | |
|---|---|
| **Laser parameters** | |
| Laser type | Nd:YAG |
| Wavelength | 213 nm |
| Spot diameter | 80 μm |
| Scan speed | 80 μm $s^{-1}$ |
| Line spacing | 80 μm |
| Laser power | ~0.15 J $cm^{-2}$ |
| Frequency | 20 Hz |
| **ICP** | |
| RF power | 1200 W |
| Plasma gas flow rate | 15 L $min^{-1}$ |
| Carrier gas flow rate | 1.15 L $min^{-1}$ |
| Sampling depth | 4 mm |
| Scanning mode | Peak hoping, time resolved analysis |
| Sampling cone | Pt, Ni base |
| Skimmer cone | Pt, Ni base |

stable throughout the entire experiment, indicating that the formation of matrix-based $^{40}Ar^{16}O^+$ was negligible.

Images for *m*/*z* 63 and 65, corresponding to the two natural isotopes of Cu are shown in Fig. 1c. $^{63}Cu^+$ was potentially interfered by $^{40}Ar^{23}Na^+$, $^{40}Ca^{23}Na^+$ and $^{31}P^{16}O_2{}^+$, and $^{65}Cu^+$ by $^{40}Ar^{25}Mg^+$. Droplet 'Int' contained 10 mg $kg^{-1}$ of both $^{31}P$ and $^{25}Mg$, and droplet A1 contained 10 mg $kg^{-1}$ $^{40}Ca$. No signal was recorded for *m*/*z* 63 or 65 in these ablated droplets. This indicated that Ar- or O-based polyatomic interferences were below the instrument's limit of detection, and the Pearson's correlation coefficient was 0.954 for the resulting images.

Further investigation of the influence of polyatomic interferences was carried out by examining the abundance ratios of elements with two measurable isotopes (Table 4). Close correlation between each element's natural isotopic abundance and measured uncorrected abundance ratios were confirmed. While the sequential mass analyser in a quadrupole ICP-MS is more prone to intrinsic uncertainty due to the mode of detection when compared to multicollector designs as heavier isotopes are more efficiently transmitted and detected,[28] our data was either within or close to the measured uncertainty expected for a quadrupole analyser. This comparison clearly demonstrated polyatomic interferences on the abundance ratio were negligible.

These data support the use of continued use of LA-ICP-MS for interference-free imaging applications in the biological sciences, showing that the most commonly expected matrix-based species arising from highly abundant elements such as Na, K, P and O are absent using typical LA-ICP-MS operating procedures, in contrast to that which was previously claimed but not experimentally demonstrated.[29] We have previously discussed the utility of reaction gases, such as hydrogen (in an octopole-equipped ICP-MS)[30] and oxygen (for mass-shifting using triple quadrupole-design ICP-MS systems),[31] though in both cases gases were used for either improving signal to noise ratios for extremely small sample volumes or low-abundance elements such as Se, respectively.

Table 4 Isotopic abundance patterns for analysed elements with multiple isotopes

| Isotopes | Natural abundance ratio | Uncorrected abundance ratio |
|---|---|---|
| $^{24}Mg^+/^{26}Mg^+$ | 7.17 | 6.89 ± 0.07 |
| $^{43}Ca^+/^{44}Ca^+$ | 0.06 | 0.06 ± 0.01 |
| $^{56}Fe^+/^{57}Fe^+$ | 43.3 | 41.5 ± 0.22 |
| $^{63}Cu^+/^{65}Cu^+$ | 2.24 | 2.09 ± 0.01 |
| $^{64}Zn^+/^{66}Zn^+$ | 1.74 | 1.67 ± 0.01 |
| $^{95}Mo^+/^{98}Mo^+$ | 0.66 | 0.62 ± 0.01 |
| $^{111}Cd^+/^{114}Cd^+$ | 0.45 | 0.43 ± 0.01 |

# 4 Conclusions

Ablation of micro-volume dried droplets did not produce a detectable amount of interfering polyatomic species. Dry plasma conditions, lower plasma power and shorter sample depth was adequate for limiting the formation of matrix-based and spectral interferences. Natural isotopic abundance patterns were confirmed. The suitability of LA-ICP-MS for detection of sub-nanogram amounts of material was also demonstrated.

# Conflict of interest

Fred Fryer is a paid employee of Agilent Technologies Australia.

# Acknowledgements

This work was supported by the Australian Research Council's Linkage Projects program (LP120200081) with Agilent Technologies and ESI Ltd.

# Notes and references

1 A. L. Gray, *Analyst*, 1985, **110**, 551–556.
2 D. J. Hare, E. J. New, M. D. de Jonge and G. McColl, *Chem. Soc. Rev.*, 2015, **44**, 5941–5958.
3 C. Pickhardt, H.-J. Dietze and J. S. Becker, *Int. J. Mass Spectrom.*, 2005, **242**, 273–280.
4 S. F. Durrant, *J. Anal. At. Spectrom.*, 1999, **14**, 1385–1403.
5 S. Tanaka, N. Yasushi, N. Sato, T. Fukasawa, S. J. Santosa, K. Yamanaka and T. Ootoshi, *J. Anal. At. Spectrom.*, 1998, **13**, 135–140.
6 F. Vanhaecke, *Anal. Bioanal. Chem.*, 2002, **372**, 20–21.
7 I. Feldmann, N. Jakubowski and D. Stuewer, *Fresenius' J. Anal. Chem.*, 1999, **365**, 415–421.
8 S. F. Boulyga and J. S. Becker, *J. Anal. At. Spectrom.*, 2002, **17**, 1202–1206.
9 N. Jakubowski, L. Moens and F. Vanhaecke, *Spectrochim. Acta, Part B*, 1998, **53**, 1739–1763.
10 T. Hirata and Z. Miyazaki, *Anal. Chem.*, 2007, **79**, 147–152.
11 F.-X. D'Abzac, A.-M. Seydoux-Guillaume, J. Chmeleff, L. Datas and F. Poitrasson, *J. Anal. At. Spectrom.*, 2012, **27**, 108–119.
12 R. E. Russo, X. Mao, H. Liu, J. Gonzalez and S. S. Mao, *Talanta*, 2002, **57**, 425–451.

13 G. P. Jackson, F. L. King and D. C. Duckworth, *J. Anal. At. Spectrom.*, 2003, **18**, 1026–1032.
14 N. Shibata, N. Fudagawa and M. Kubota, *Spectrochim. Acta, Part B*, 1993, **48**, 1127–1137.
15 L. Yang, R. E. Sturgeon and Z. Mester, *Anal. Chem.*, 2005, **77**, 2971–2977.
16 D. Günther, H. Cousin, B. Magyar and I. Leopold, *J. Anal. At. Spectrom.*, 1997, **12**, 165–170.
17 L. Yang, R. E. Sturgeon and Z. Mester, *J. Anal. At. Spectrom.*, 2005, **20**, 431–435.
18 P. Grinberg, L. Yang, Z. Mester, S. Willie and R. E. Sturgeon, *J. Anal. At. Spectrom.*, 2006, **21**, 1202–1208.
19 J. V. Cizdziel, *Anal. Bioanal. Chem.*, 2007, **388**, 603–611.
20 M. Bonta, B. Hegedus and A. Limbeck, *Anal. Chim. Acta*, 2016, **908**, 54–62.
21 M. Grehn, T. Seuthe, M. Höfner, N. Griga, C. Theiss, A. Mermillod-Blondin, M. Eberstein, H. Eichler and J. Bonse, *Opt. Mater. Express*, 2014, **4**, 689–700.
22 P. E. Dyer, D. M. Karnakis, P. H. Key and P. Monk, in *Laser ablation*, ed. E. Fogarassy, D. Geohegan and M. Stuke, Elsevier, 1996.
23 D. J. Hare, B. Reedy, R. Grimm, S. Wilkins, I. Volitakis, J. L. George, R. A. Cherny, A. I. Bush, D. I. Finkelstein and P. Doble, *Metallomics*, 2009, **1**, 53–58.
24 C. Austin, F. Fryer, J. Lear, D. Bishop, D. J. Hare, T. Rawling and P. Doble, *J. Anal. At. Spectrom.*, 2011, **26**, 1494–1501.
25 Q. Li, A. Lau, T. J. Morris, L. Guo, C. B. Fordyce and E. F. Stanley, *J. Neurosci.*, 2004, **24**, 4070–4081.
26 T. W. May and R. H. Wiedmeyer, *At. Spectrosc.*, 1998, **19**, 150–155.
27 J. P. Bernal, S. M. Eggins and M. T. McCulloch, *J. Anal. At. Spectrom.*, 2005, **20**, 1240–1249.
28 J. R. Encinar, J. I. G. Alonso, A. Sanz-Medel, S. Main and P. J. Turner, *J. Anal. At. Spectrom.*, 2001, **16**, 315–321.
29 J. S. Becker, A. Matusch and B. Wu, *Anal. Chim. Acta*, 2014, **835**, 1–18.
30 J. Lear, D. J. Hare, F. Fryer, P. A. Adlard, D. I. Finkelstein and P. A. Doble, *Anal. Chem.*, 2012, **84**, 6707–6714.
31 D. P. Bishop, D. Clases, F. Fryer, E. Williams, S. Wilkins, D. J. Hare, N. Cole, U. Karst and P. A. Doble, *J. Anal. At. Spectrom.*, 2016, **31**, 197–202.